

# Development of Titanium Surgery Implants for Improving Osseointegration Through Formation of a Titanium Nanotube Layer

N. A. Al-Mobarak\*, A. A. Al-Swayih

Department of Chemistry, College of Science, Princess Nora Bint Abdul Rahman University,  
Box:22559, Riyadh 11416, Kingdom of Saudi Arabia

\*E-mail: [N\\_Almobarak@yahoo.com](mailto:N_Almobarak@yahoo.com)

*Received:* 3 September 2013 / *Accepted:* 21 October 2013 / *Published:* 15 November 2013

---

Recently, titanium and titanium alloys with nanotube layers by anodizing process have gained great interests as surgical implant materials. In this paper, the electrochemical stability of TiO<sub>2</sub> nanotube layers prepared by anodization of pure Ti in three solutions has been investigated in simulated biological environment by use of open-circuit potential (OCP), electrochemical impedance spectroscopy (EIS) and potentiodynamic polarization (PD) tests. The PD testing results indicate that the nanotubular Ti shows a slightly higher passivation current than the mechanically polished titanium in Hank's solution, this is attributed to the large surface area created by the nanostructure. Moreover, the electrochemical stability of Ti nanotubes is enhanced, as judged by the more nobler open circuit potential values compared to that of Ti. The dependence of the electrochemical stability of the nanotubular surface depended on the dimensions of the TiO<sub>2</sub> nanotube which was controlled by optimizing the anodization electrolyte composition. The results reveal that architecting the surface of titanium on the nanoscale render the surface more biocompatible by creating large surface area and more sustainable by providing more stabilized surface which is less vulnerable to corrosion. .

---

**Keywords:** Titanium nanotube, anodization, TiO<sub>2</sub>, surgery implants

## 1. INTRODUCTION

Ti and Ti alloys are the materials of choice for most dental and orthopedic applications. The many advantages of these materials include biocompatibility, good resistance to corrosion, low density and sufficiently strong for use as orthopedic implant materials [1]. These properties have been attributed to the natural oxide layer formed spontaneously on Ti surface [2]. The natural oxide is thin (about 3–8 nm in thickness), amorphous, and stoichiometrically defective. It is well known that the

protective and stable oxides on titanium surfaces provide favorable osseointegration. The stability of this titanium oxide layer depends strongly on its composition, structure and thickness. As a consequence, great efforts have been devoted to thickening and stabilizing the surface oxide on titanium to achieve the desired biological response. Various methods were used to improve the interfacial properties and clinical lifetime of Ti-based implants [3].

Surface treatments such as roughening by sand blasting, formation of anatase phase TiO<sub>2</sub> [4], hydroxyapatite coating, or chemical treatment [4-9] have been utilized to further improve the bioactivity of Ti and enhance bone growth [10]. One method among them is anodization, which induced the formation of rough and porous TiO<sub>2</sub> surfaces [11]. Presently anodization is one of the most commonly used methods to produce nanoporous surface, due to its simplicity and feasibility. In addition, the size and shape of nanostructured materials can be tuned to the desire dimension [2].

The titanium with nanotube layers cannot only significantly increase osteoblast or bone forming cell adhesion and function in vitro [12-14], but also promote in vivo bone formation around implants compared to their unanodized counter parts [15,16]. This nanotube titanium layer plays an important role in the enhancement of osseointegration through the improvement of the adhesion of the hydroxyapatite (HAP) coating that is deposited onto TiO<sub>2</sub> [17]. Oh et al. [12] indicated that the cell adhesion could be improved by up to 400% because of the mechanical interlocking between the HAP coating and the nanotube titanium oxide layer.

The TiO<sub>2</sub> nanotube films have been extensively explored as adhesion and growth support platforms for bone and stem cells, for the prevention of bacterial adhesion, drug delivery and enhancing blood clotting for control of haemorrhage [18–21]. Favourable bone cell growth, cell differentiation, and apatite-forming abilities were recently demonstrated on implants with nanotubular titania surfaces demonstrating its promise for bone implants [22]. Recently development in stem cell research demonstrated that titania nanotubes are able to differentiation of mesenchymal stem cells into specific cells (osteoblasts) [23,24]. Furthermore, the outstanding photocatalytic properties of the nanotube surface were applied to photo-induced killing of cancer cells which suggests a possible application of nanotubes for an anticancer treatment [25].

However, up to now, few articles about corrosion behavior of nanotubes have been published [26-28]. Corrosion is the most decisive property for the biocompatibility of an implant. The present work was addressed to test corrosion behavior of titanium with different diameter nanotube layers in Hank's solution and detected by scanning electron microscope (SEM), electrochemical impedance spectroscopy (EIS) and potentiodynamic polarization. This study aims to enhance the understanding of corrosion characteristics of different nanotubes on titanium in physiological environment.

## 2. MATERIALS AND METHODS

### 2.1. TiO<sub>2</sub> nanotube layer formation

Ti foils with an area of 20 mm x 30 mm and thickness of 0.25 mm (99.5% metal basis, Alfa Aesar) were used as starting material in order to obtain the TiO<sub>2</sub> nanotube arrays. A preliminary

treatment was performed by degreasing the Ti foils using sonication in acetone, in isopropanol, and, finally, in methanol. The foils were subsequently rinsed with deionized water and dried in nitrogen stream. TiO<sub>2</sub> nanotube arrays were formed by anodization in different solution at 20 V for 30 min. The three solutions used for nanotube preparation were: (T1) 1M Na<sub>2</sub>SO<sub>4</sub> + 0.5 wt.% NaF, (T2) 1.0 M H<sub>3</sub>PO<sub>4</sub> + 0.8 wt.% NaF and (T3) 0.5 (wt) % HF. Following this, the anodized samples were rinsed with deionized water and dried in nitrogen stream. For comparison, a fresh sample of Ti without nanotube (T) were studied. Table 1 lists the samples and conditions used in this study.

**Table 1.** Summary of conditions of anodization

Sample	Electrolyte composition in anodization	voltage	time
T	-	-	-
T1	1M Na <sub>2</sub> SO <sub>4</sub> + 0.5 wt.% NaF	20 V	30 min
T2	1.0 M H <sub>3</sub> PO <sub>4</sub> + 0.8 wt.% NaF		
T3	0.5 (wt) % HF		

## 2.2. Surface characterization

The surface morphology of the TiO<sub>2</sub> nanotube arrays was characterized using a scanning electron microscope (Jeol JSM-7600F Field-Emission Scanning Electron Microscope).

## 2.3. Electrochemical tests

All electrochemical measurements were performed at 37 °C in s Hank's physiological solution (8 g/l NaCl, 0.4 g/l KCl, 0.35 g/l NaHCO<sub>3</sub>, 0.25 g/l NaH<sub>2</sub>PO<sub>4</sub>.×H<sub>2</sub>O, 0.06 g/l Na<sub>2</sub>HPO<sub>4</sub>.2H<sub>2</sub>O, 0.19 g/l CaCl<sub>2</sub>.2H<sub>2</sub>O, 0.19 g/l MgCl<sub>2</sub>, 0.06 g/l MgSO<sub>4</sub>.7H<sub>2</sub>O and 1 g/l glucose, pH 7.8) [29-32].

A conventional three-electrode electrochemical cell system was used. Saturated calomel electrode (SCE) and platinum mesh were used as reference and counter electrodes, respectively. Potentials in the text refer to the SCE scale.

In the experiments, the open circuit potential (OCP) was measured for an hour. Then, electrochemical impedance spectroscopy (EIS) was recorded. The frequency ranged from 100 kHz to 10 mHz at 10 cycles per decade, with an ac amplitude of ±10 mV. The absolute impedance and phase angle were measured at each frequency. The impedance data were interpreted on the basis of equivalent electrical circuits, using the Zsim program for fitting the experimental data. In potentiodynamic polarization (PD) tests, the working electrode potential is continuously increased from -250 to 500 mV relative to the OCP at a scan rate of 1 mV/s.

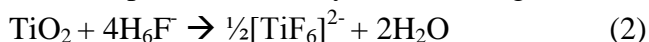
### 3. RESULTS AND DISCUSSION

#### 3.1. The formation of nanotube oxide layers and the morphology of surfaces

It is generally agreed that the formation of TiO<sub>2</sub> nanotube arrays in a fluoride containing electrolyte is the result of two competing electric field-assisted processes [33,34]. The first process is the oxidation of the Ti metal to form a passive TiO<sub>2</sub> layer [35]:



Due to the fluoride ions presence, the second process is the chemical dissolution of the formed TiO<sub>2</sub> oxide with pits formation by the following reaction [35,36]:



These pits act as the pore forming centres; as was described in the literature [37]. This model of dissolution is a key factor of well organized structure of titanium nanotubes [36].

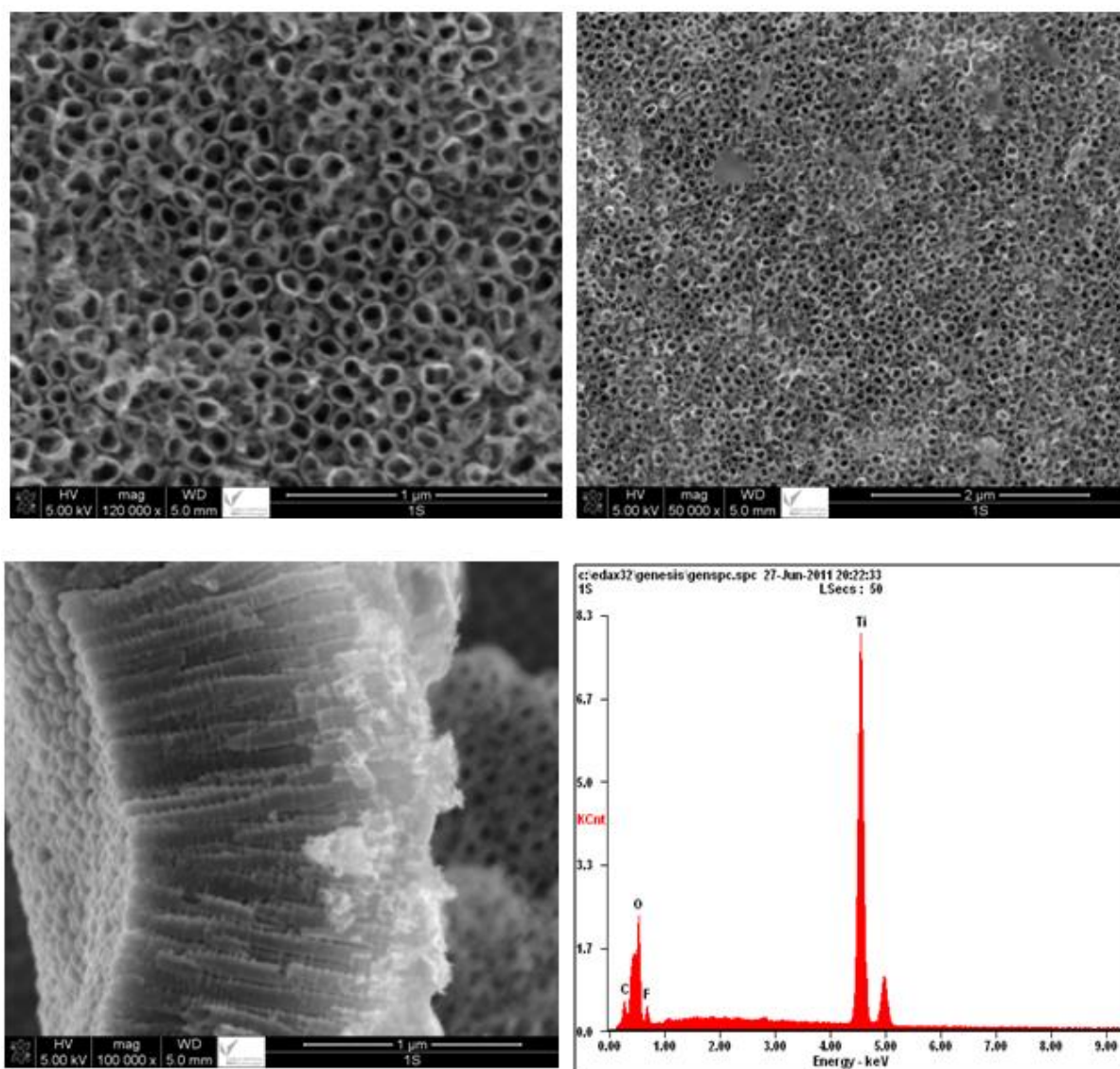


**Figure 1.** The SEM images and EDX of titanium oxide nanotubes formed on sample T1

Fig. 1 shows SEM images of the resulting layer for sample T1, which formed in 1M Na<sub>2</sub>SO<sub>4</sub> containing 0.5 wt.% NaF. The figure revealed that the resulting layer consists of self-organized nanotubes with the average diameters of approx. 70 nm and a length of approx. 1.2 μm. It is apparent that the nanotubes are open on the top. This morphology was reported before for p-TiO<sub>2</sub> films formed in SO<sub>4</sub><sup>2-</sup> containing solutions [38,39]. The closed bottoms correspond to the barrier layers formation, similar to the case of porous alumina [40].

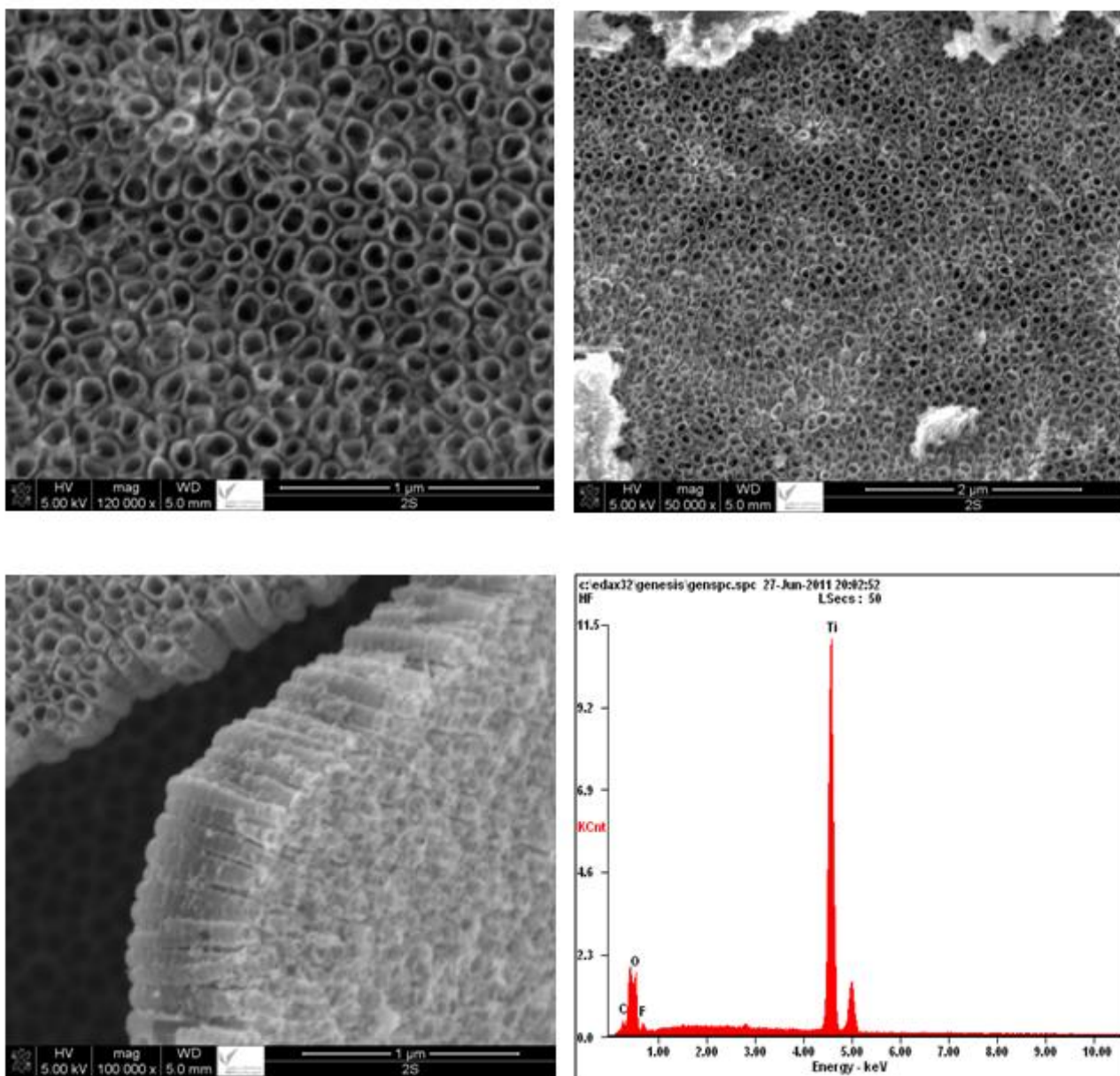


**Figure 2.** The SEM images and EDX of titanium oxide nanotubes formed on sample T2

Fig. 2 shows SEM images for the second sample T2, which shows self-organized TiO<sub>2</sub> nanotubes formed in the phosphate electrolyte containing small amount of fluoride ions. A key reason to study phosphate electrolytes is that typically compact anodic films formed on Ti contain a

significant amount of phosphorous species [41]. This anion uptake may modify the functional properties not only of the compact oxide layers but even more, the properties of the porous layer [40]. From fig. 2, the resulting nanotube layer has average diameters of approx. 93 nm and a length of approx. 536 nm.

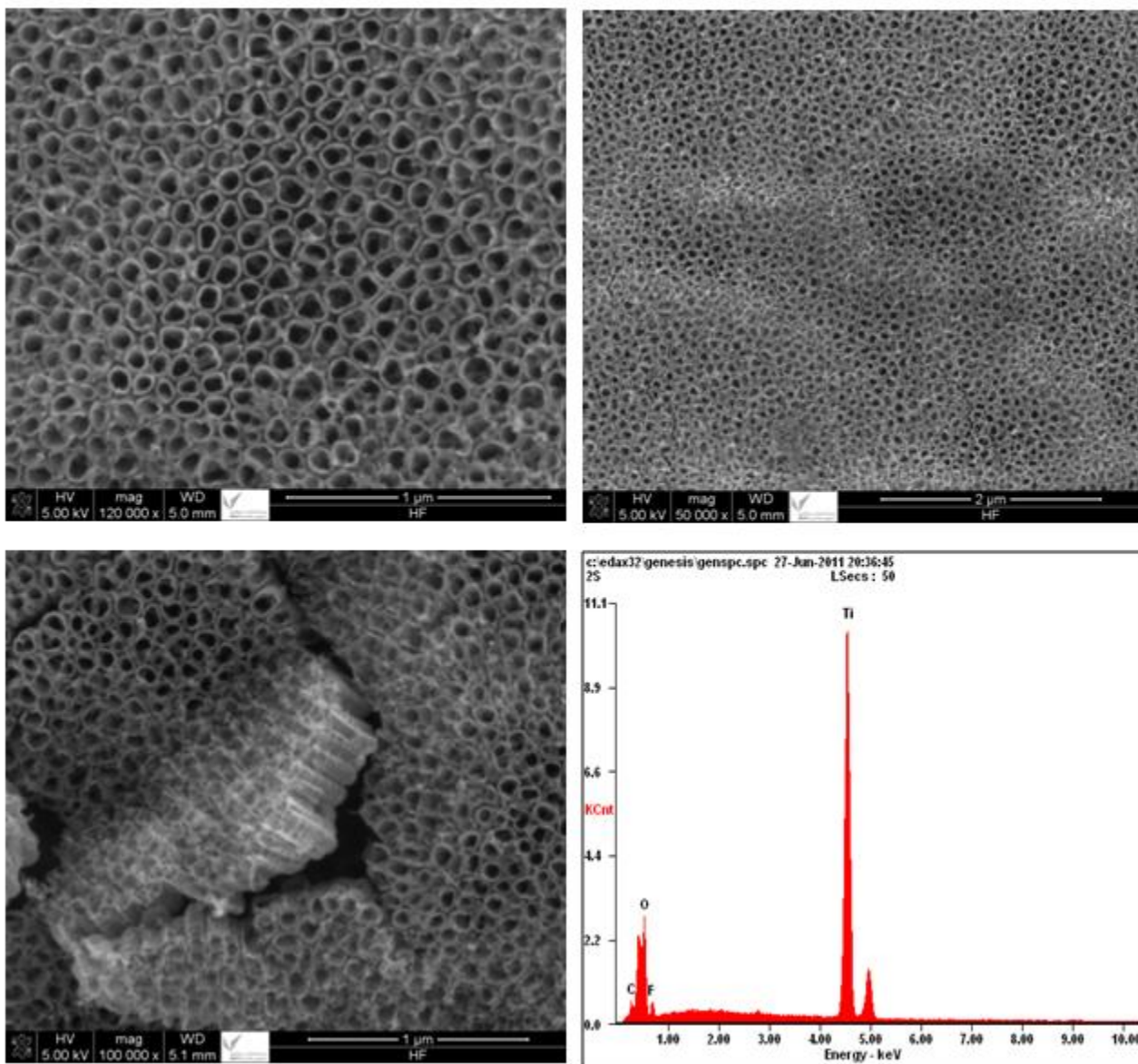


**Figure 3.** The SEM images and EDX of titanium oxide nanotubes formed on sample T3

Fig. 3 shows SEM images for the third sample, which formed in HF solution. The images reveal that the layer of titanium nanotube with average diameters of approx. 52 nm and a length of approx. 250 nm. The longer nanotubes were formed in sample T1, while the shorter were formed in sample T3. In addition, the smallest average diameters of the nanotubes were observed in sample T3. The nano-architecture of the surface may strongly affect the electrochemical properties of the samples.

### 3.2. Open circuit potential measurements:

Fig. 4 presents the time-variation of the open circuit potential (OCP) for titanium and titanium nanotubes-coated samples. The immersion potentials of titanium samples with nanotube oxide are nobler than that of titanium. The OCP curves show that the potential of T1 shifted positively, then moves to more negative values. For T2 and T3, the OCP reached a steady state during the first minutes of the test. The gradual decrease in the OCP values for T1 sample indicates that the equilibrium between chemical dissolution and rebuilding of the oxide film is not completely established during this immersion period. On the other hand, the OCP of the nanotubular sample T2 and T3 is stable after the initial shift, indicating an equilibrium between the formation and dissolution of surface oxide on the nanotubes is established [42,43].

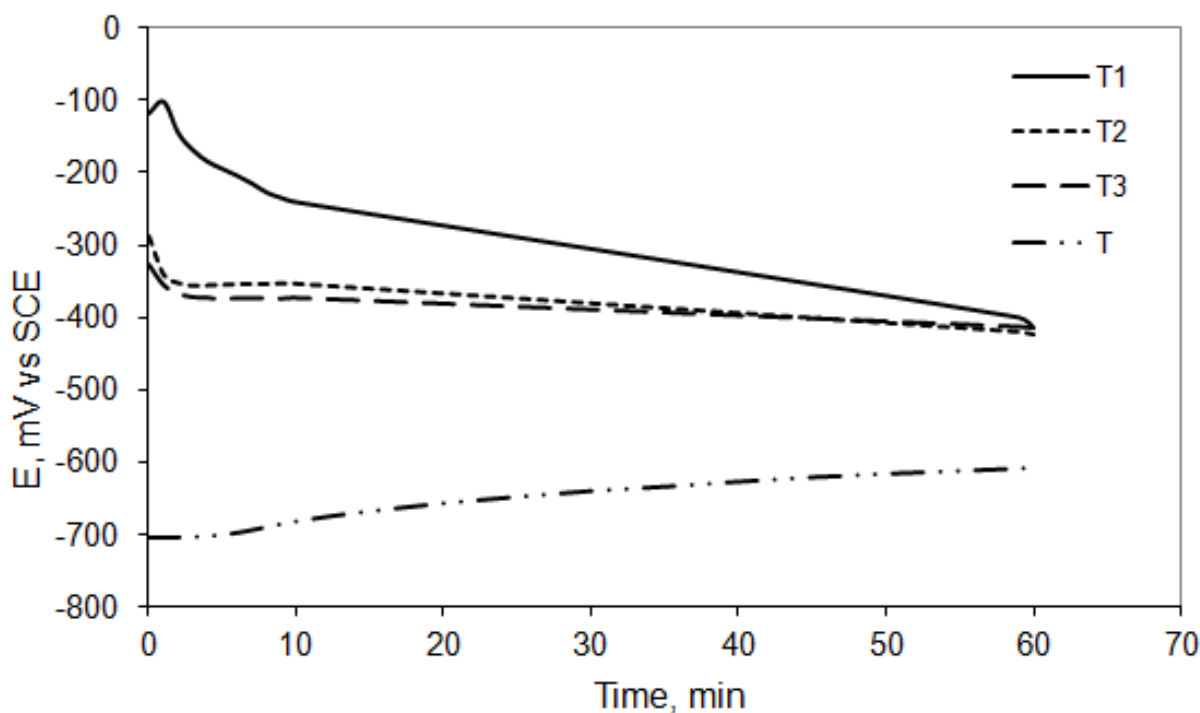


**Figure 4.** The OCPs of Ti and nanotube Ti samples in Hank's solution for one hours

The OCP of T in the test solutions rose rapidly and then gradually reached a stable value. This is because a titanium oxide film began to grow and thickens after the sample was immersed in the solution, which resulted slight improvement in corrosion resistance and a relatively stable state [28,44-45].

The values of OCP after 1 hour of immersion are similar for nanotubes-coated samples. Compared to T specimen, the OCP of the TiO<sub>2</sub> nanotubular layers is more positive, demonstrating better electrochemical stability in Hank's solution, as reported by Liu et al [43].

### 3.3. Potentiodynamic Polarization measurements:

Fig. 5 shows the variation of current density with potential for different samples immersed in Hank's solution. Under these conditions, the reactions occurring at the anode is generally the anodic oxidation of Ti and at high potential is the oxygen evolution (water oxidation). At the same time, on the cathode (the counter electrode), the cathodic reaction is the hydrogen evolution ( $2\text{H}^+ + 2\text{e} = \text{H}_2$ ). If, on the anode surface a protecting, generally low conducting, passive film is present, this results in retardation of the electrons conduction across the film and hence a break in the current is observed eventhough the potential is increasing. Inspection of the curves of Fig. 2 we can note that, generally, the samples show immediate passivation behavior in the anodic polarization region. During this passive region, titanium is protected by forming a  $\text{TiO}_2$  layer that results from anodic oxidation of titanium [35]. The reaction is expressed by equation (1) and the stability of this layer is justified by the low value of free energy of formation of  $\Delta G_{298}^\circ = -820$  kJ/mol. The layer retard electronic conduction and consequently shows a break in the current. On the other hand, the titania nanotubes (TiNT) protected samples are expected to have a similar break in the current, however the fact that they have much high surface area accommodating more electrolyte and reaction surface explains the higher passivation current observed. On referring to Fig. 4, the values of  $E_{\text{corr}}$  of these samples are nobler than that of bare titanium which emphasizes the shielding effect to the underlying surface rendering it less vulnerable for corrosion. The observable differences in the behavior of samples T1-T3 is attributed to the surface nano-architectures. On referring to SEM images of the surfaces of samples T1, T2 and T3 in Figs. 1, 2 and 3 respectively, we note that the surface of T3 looks more uniform, narrower tube mouths, shorter lengths, and almost no debris. This gives sample T3 the virtue of more capability for better passivation behavior. The result emphasizes on the important role in selecting the proper electrolyte for anodizing titanium for the purpose of potential use as biomaterial. In which a large surface area, inertness of the surface and less detachable debris on the surface is required. The large surface area enhances more cells or protein adsorption, the inertness means less corrosion susceptibility, and less detachable debris that possibly detaches to human fluid leading to possible contamination and/or inflammation.

This results are consistent to pre-researched results of some titanium alloys [46,47]. The results of corrosion potential ( $E_{\text{corr}}$ ), corrosion current density ( $I_{\text{corr}}$ ) from the polarization curves are given in Table 2. As for corrosion data acquired from the potentiodynamic polarization curves, the T3 exhibited lower current density than than that of T1 and T2 surfaces. This may be due to an immediate and effective passivation on the T3 surface [27]. But current density for T1 is greater than for the T, which means lower corrosion resistance for the nanotubes compared to Ti. Saji et al. [26] also found this phenomenon when studying corrosion characteristic of nanotubular oxide on Ti-35Nb-5Ta-7Zr alloy in Ringer's solution, and Yu et al. found the same results for some titanium alloys [28]. They thought it was the tube bottom interface shaped by distinctly separated barrier oxide/concave that contributed to the lower corrosion resistance of the nanotubes. Our nanotubes also formed the similar interface, which seem to be a reason for lower corrosion on nanotube samples.

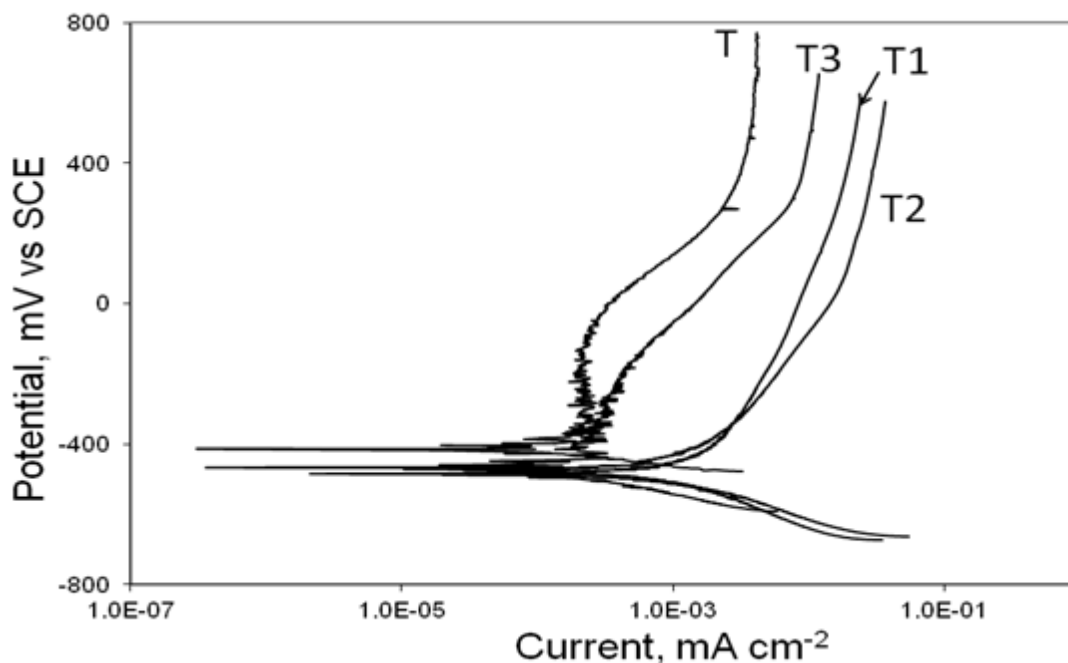


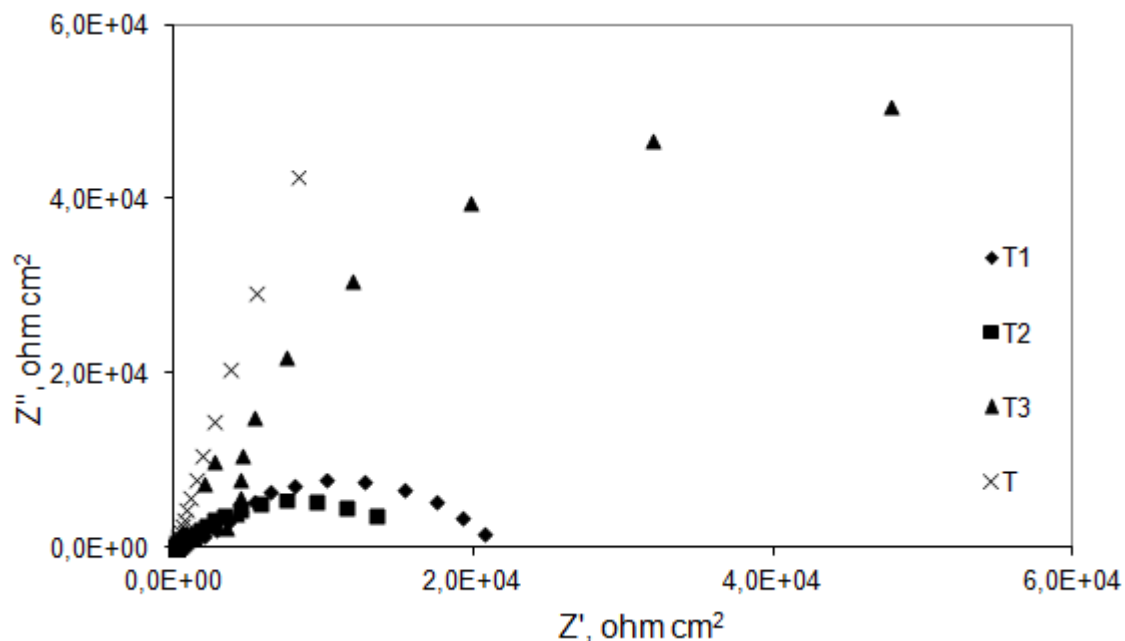
Figure 5. Potentiodynamic polarization plots of Ti and nanotube Ti samples in Hank's solution

Table 2. Electrochemical parameters obtained from potentiodynamic polarization test

Sample	$E_{corr}$ V	$B_a$ mV dec <sup>-1</sup>	$B_c$ mV dec <sup>-1</sup>	$I_{corr}$ mA cm <sup>-2</sup>
T1	-0.482	296	131	$1.01 \times 10^{-3}$
T2	-0.472	249	155	$1.17 \times 10^{-3}$
T3	-0.484	178	189	$8.56 \times 10^{-4}$
T	-0.337	461	101	$8.18 \times 10^{-5}$

### 3.4. EIS analysis

Fig. 6 shows the Nyquist plots ( $-Z_{imag}$  vs.  $Z_{real}$ ) acquired from Ti and Ti nanotube specimens. The impedance spectra are fitted with ZSimp Win software using two equivalent circuits. According to literature [48-50] the film on Ti is composed of a bi-layered oxide consisting of a porous outer layer and a barrier inner layer, which can be interpreted by using two time constants  $R_s(R1Q1(R2Q2))$ , Fig. 7(a), where  $R_s$  corresponds to the resistance of the solution,  $R1$  corresponds to the resistance of the porous layer,  $R2$  corresponds to the resistance of the barrier layer,  $Q1$  relates to the capacitance of the porous layer and  $Q2$  is the capacitance of the barrier. A constant-phase element representing a shift from the ideal capacitor was used instead of the capacitance itself, for simplicity. The impedance of a phase element is defined as  $Z_{CPE} = [C(j\omega)\alpha]^{-1}$ , where  $-1 \leq \alpha \leq 1$ . The value of  $\alpha$  is associated with the non-uniform distribution of current as a result of roughness and surface defects layer.



**Figure 6.** Nyquist diagrams of Ti and nanotube Ti samples at the open-circuit potential

**Table 3.** Fitted electrochemical parameters determined from the Nyquist spectra based on the equivalent circuits

Sample	$R_s$ ohm $cm^2$	$R_1 \times 10^3$ ohm $cm^2$	$Q_1 \times 10^{-4}$ F $cm^{-2}$	$n_1$	$R_2 \times 10^3$ ohm $cm^2$	$Q_2 \times 10^{-4}$ F $cm^{-2}$	$n_2$
T	42.9	77.9	0.021	0.96	909.0	0.0165	0.85
T1	56.2	14.2	2.11	0.95	42.0	1.76	0.89
T2	43.1	7.95	3.06	0.94	36.8	2.11	0.91
T3	86.1	31.3	1.91	0.96	272.0	0.768	0.90

The titania nanotube-coated sample consists of an outer nanotube layer and an inner barrier layer [42]. The EIS spectra are interpreted by using a model with two constants  $R_s(R_1Q_1)(R_2Q_2)$ , as shown in Fig. 7(b), where  $R_1$  represents the resistance of the outer nanotube layer,  $Q_1$  is the constant phase element of the outer nanotube layer,  $R_2$  is the resistance of the inner barrier layer, and  $Q_2$  is corresponding to the inner barrier layer [27,47]. The electrochemical parameters by fitting the circuits (error of less than 10%) are presented in Table 3.

The values of  $R_2$  indicate that the samples with nanotube  $TiO_2$  layer have high corrosion resistance. However, with smallest  $TiO_2$  nanotube diameters, for T3, the corrosion resistance  $R_2$  is higher than the other two samples, which disclosing the effects of the nanotube diameter on the corrosion resistance.

Based on these results, both the length and diameter of the nanotube might affect the electrochemical corrosion behavior of  $TiO_2$  nanotubes atop the surface of titanium foil. The wall between  $TiO_2$  nanotubes may be another important factor influencing the electrochemical stability [43].

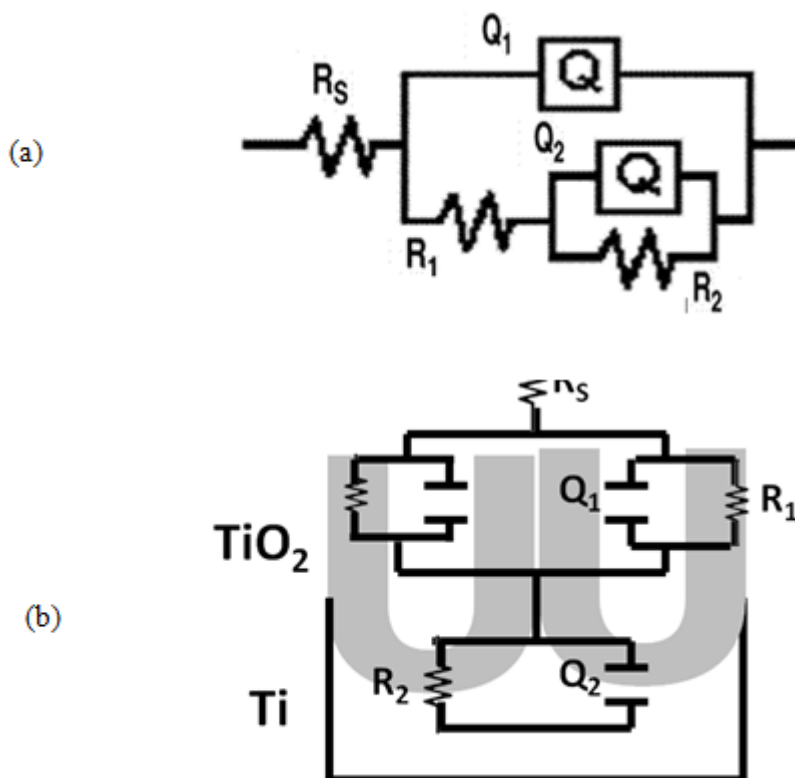


**Figure 7.** Equivalent circuit used to model impedance spectra: (a) of the nanotube sample, (b) of titanium

The corrosion behavior of Ti depends on the interaction between the oxide film and surrounding electrolyte [51]. Therefore, the difference in the corrosion resistance may be attributed to their different microstructure of the surface oxide layer. The mechanically polished surface exhibits two time constants corresponding to the presence of a highly capacitive behavior of the compact passive barrier layer and an outer porous layer. In comparison, the plots of the nanotubes indicate two time constants corresponding to the presence of two interfaces, a highly corrosion resistant barrier layer and the outer nanotubular layer. Upon exposure of Ti to air, a thin and stable oxide, several nanometers thick, is formed on its surface [52]. In contrast, the anodization process results in the growth of uniform arrays atop the titanium foils in the fluoride solutions and an electrically insulating barrier layer separating the nanotubes from the conducting titanium foil. The diameter of  $\text{TiO}_2$  nanotube depends on the anodization conditions [53].

The EIS results in Table 3 indicate that the  $R_1$  values of T are higher than that of nanotube samples. Moreover,  $R_2$  magnitudes are highest for T3 compared to the values of T1 and T2. Therefore, the barrier layer formed during anodizing process in HF solution provides more effective corrosion protection, as shown by the higher  $E_{\text{corr}}$  and lower corrosion current density in Table 2. This behavior of T3 can be attributed to the well-structured surface the oxide nanotube/barrier layers coupled with uniformity. The larger pore diameter in the  $\text{TiO}_2$  nanotube array introduces a larger effective exposed area in close proximity with the electrolyte thus enabling diffusion of corrosive ions in the electrolyte [54,55]. The diameter of the  $\text{TiO}_2$  nanotubes in T3 is smaller than that of T1 and T2. The interface

reaction is enhanced by a larger exposed area between the surface and electrolyte. The larger nanotubes provide more channels for the electrolyte to reach the barrier layer consequently increasing the chance of the reaction between corrosive ions and titanium oxide [51,56]. The phenomenon is similar to the results reported by Jang and Kim who used nanotubes approximately 150–200 nm and 220 nm in size, respectively in the corrosion tests [42,56]. Based on these results, both the thickness of the barrier layer and diameter of the nanotube might affect the electrochemical corrosion behavior of TiO<sub>2</sub> nanotubes atop the surface of titanium foil. The wall between TiO<sub>2</sub> nanotubes may be another important factor influencing the electrochemical stability [43].

From the standpoint of osseointegration, TiO<sub>2</sub> nanotubes enhance apatite formation in biomedical applications compared with the Ti metal [10] or flat TiO<sub>2</sub> layer [57]. The nanotubular structure (influenced by pore structure and pore size) contains significantly increased surface area and also more ‘in between - nanotube pathways for fluid’ [10]. The increased surface area of the TiO<sub>2</sub> nanotubes is useful for accelerated bone growth in orthopedic/dental applications [10,58].

#### 4. CONCLUSION

TiO<sub>2</sub> nanotubes with different sizes are synthesized on Ti by the anodization process in different solutions containing fluoride ion. The nanotubes coated samples show higher open-circuit potentials than mechanically polished Ti in Hank's solution. The EIS and PD results indicate that the electrochemical stability of the nanotubular surface depends on the diameter of the TiO<sub>2</sub> nanotube. A diameter that is large leads to decreased corrosion resistance. Our results exhibit that the titanium with nanotubes can improve the osseointegration of surgical implants in physiological environment.

#### ACKNOWLEDGMENT

The authors gratefully acknowledge the financial aid from the Deanery of Scientific Research of the University of Princess Norah bint Abdulrahman, Riyadh, Kingdom of Saudi Arabia to the Research Project number 026-K-32.

#### References

1. A. Bigi, E. Boanini, B. Bracci, A. Facchini, S. Panzavolta, F. Segatti, L. Sturba, *Biomaterials* 26 (2005) 4085.
2. K. Indira, U. Kamachi Mudali, N. Rajendran, *Ceramics International* 39 (2013) 959.
3. Seung-Hyun Jang, Han-Cheol Choe, Yeong-Mu Ko, William A. Brantley, *Thin Solid Films* 517 (2009) 5038.
4. M. Uchida, H.M. Kim, T. Kokubo, S. Fujibayashi, T. Nakamura, *J. Biomed. Mater. Res.* 64 (2003) 164.
5. E. Lugscheider, T. Weber, M. Knepper, F. Vizethum, *Mater. Sci. Eng., A Struct. Mater.: Prop. Microstruct. Process.* A139 (1991) 45.
6. P. Ducheyne, W. Van Raemdonck, J.C. Heughebaert, M. Heughebaert, *Biomaterials* 7 (1986) 97.
7. D.R. Cooley, A.F. Van Dellen, J.O. Burgess, A.S. Windeler, *J. Prosthet. Dent.* 67 (1992) 93.
8. M.C. De Andrade, M.S. Sader, M.R.T. Filgueiras, T. Ogasawara, *J. Mater. Sci., Mater. Med.* 11 (2000) 751.
9. H.M. Kim, F. Miyaji, T. Kokubo, T. Nakamura, *J. Biomed. Mater. Res.* 32 (1996) 409.
10. Seunghan Oh, Sungho Jin, *Materials Science and Engineering C* 26 (2006) 1301.
11. A. Ghicov, P. Schmuki, *Chemical Communications* 20 (2009) 2791.

12. S. Oh, C. Daraio, L.H. Chen, T.R. Pisanic, R.R. Finones, S. Jin, *J. Biomed. Mater. Res. A*, 78 (2006) 97.
13. K.C. Popat, L. Leoni, C.A. Grimes, T.A. Desai, *Biomaterials* 28 (2007) 3188.
14. C. Yao, E.B. Slamovich, T.J. Webster, *J. Biomed. Mater. Res. A* 85 (2008) 157.
15. C. von Wilmsowky, S. Bauer, R. Lutz, M. Meisel, F.W. Neukam, T. Toyoshima, P. Schmuki, E. Nkenke, K.A. Schlegel, *J. Biomed. Mater. Res. B: Appl. Biomater.* 89 (2009) 165.
16. L.M. Bjursten, L. Rasmusson, S. Oh, G.C. Smith, K.S. Brammer, S. Jin, *J. Biomed. Mater. Res. A*, 92 (2010) 1218.
17. Sepideh Minagar, Christopher C. Berndt, James Wang, Elena Ivanova, Cuie Wen, *Acta Biomaterialia* 8 (2012) 2875.
18. L. Peng, M.L. Eltgroth, T.J. LaTempa, C.A. Grimes, T.A. Desai, *Biomaterials* 30 (2009) 1268.
19. L.L. Peng, A.D. Mendelsohn, T.J. LaTempa, S. Yoriya, C.A. Grimes, T.A. Desai, *Nano Lett.* 9 (2009) 1932.
20. K.S. Brammer, S. Oh, J.O. Gallagher, S. Jin, *Nano Lett.* 8 (2008) 786.
21. K.C. Popat, M. Eltgroth, T.J. LaTempa, C.A. Grimes, T.A. Desai, *Biomaterials* 28 (2007) 4880.
22. S.H. Oh, R.R. Finones, C. Daraio, L.H. Chen, S. Jin, *Biomaterials* 26 (2005) 4938.
23. S. Oh, K.S. Brammer, Y.S.J. Li, D. Teng, A.J. Engler, S. Chien, *PNAS* 106 (2009) 2130.
24. J. Park, S. Bauer, K.A. Schlegel, F.W. Neukam, K. von der Mark, P. Schmuki, *Small* 5 (2009) 666.
25. M. Kalbacova, J.M. Macak, F. Schmidt-Stein, C.T. Mierke, P. Schmuki, *Phys. Status Solid RRL* 2 (2008) 194.
26. V.S. Saji, H.C. Choe, W.A. Brantley, *Acta Biomater.* 5 (2009) 2303.
27. W.Q. Yu, J. Qiu, L. Xu, F.Q. Zhang, *Biomed. Mater.* 4 (2009) 065012.
28. Wei-qiang Yu, Jing Qiu, Fu-qiang Zhang, *Colloids and Surfaces B: Biointerfaces* 84 (2011) 400.
29. M. H. Wong, F. T. Cheng, H. C. Man, *Appl. Surf. Sci.* 253 (2007) 7527.
30. V. Raman, S. Nagarajan, N. Rajendran, *Electrochemistry Communications* 8 (2006) 1309.
31. E. Chang, T. M. Lee, *Biomaterials* 23 (2002) 2917.
32. A. W. E. Hodgson, Y. Mueller, D. Forster, S. Virtanen, *Electrochimica Acta* 47 (2002) 1913.
33. C.A. Grimes, *J. Mater. Chem.* 17 (2007) 1451.
34. G.A. Crawford, N. Chawla, *Acta Mater.* 57 (2009) 854.
35. Xuanyong Liu, Paul K. Chu, Chuanxian Ding, *Materials Science and Engineering R* 70 (2010) 275.
36. Mihaela Mindroiu, Cristian Pirvu, Raluca Ion, Ioana Demetrescu, *Electrochimica Acta* 56 (2010) 193.
37. Y. Lai, H. Zhuanga, L. Suna, Z. Chenb, L. Changjian, *Electrochimica Acta* 54 (2009) 6536.
38. J.M. Macak, H. Tsuchiya, P. Schmuki, *Angew. Chem.* 44 (2005) 2100.
39. J.M. Macak, K. Sirotna, P. Schmuki, *Electrochimica Acta* 50 (2005) 3679.
40. Andrei Ghicov, Hiroaki Tsuchiya, Jan M. Macak, Patrik Schmuki, *Electrochemistry. Communication* 7 (2005) 505.
41. C.E.B. Marino, P.A.P. Nascente, S.R. Boaggio, R.C. Rocha-Filcho, N. Bocchi, *Thin Solid Films* 468 (2004) 109.
42. S.H. Jang, H.C. Choe, Y.M. Ko, W.A. Brantley, *Thin Solid Films* 517 (2009) 5038.
43. Chenglong Liu, Yueji Wang, Meng Wang, Weijiu Huang, Paul K. Chu, *Surface and Coatings Technology* 206 (2011) 63.
44. X. Cheng, S.G. Roscoe, *Biomaterials* 26 (2005) 7350.
45. S.L. De Assis, S. Wolyneec, I. Costa, *Electrochim. Acta* 51 (2006) 1815.
46. Han-Cheol Choe, Won-Gi Kim, Yong-Hoon Jeong, *Surface and Coatings Technology* 205 (2010) S305.
47. V.S. Saji, H.C. Choe, *Corros. Sci.* 51 (2009) 1658.
48. T. Hanawa, *Sci. Technol. Adv. Mater.* 3 (2002) 289.
49. S.Y. Yu, J. R. Scully, *Corrosion* 53 (1997) 965.

50. N.A. Al-Mobarak, A.A. Al-Swayih, F.A. Al-Rashoud, *Int. J. Electrochem. Sci.* 6 (2011) 2031.
51. A. Balamurugan, S. Rajeswari, G. Balossier, *Mater. Corros.* 59 (2008) 855.
52. S. Hiromoto, T. Hanawa, K. Asami, *Biomaterials* 25 (2004) 979.
53. S. Bauer, S. Kleber, P. Schmuki, *Electrochem. Commun.* 8 (2006) 1321.
54. D.S. Kong, *Langmuir* 24 (2008) 5324.
55. A.G. Munoz, Q. Chen, P. Schmuki, J. Solid State, *Electrochem.* 11 (2007) 1077.
56. W.G. Kim, H.C. Choe, *Trans. Nonferrous Met. Soc. China* 19 (2009) 1005.
57. H. Tsuchiya, J.M. Macak, L. Müller, J. Kunze, F.Müller, P. Greil, S.Virtanen, P. Schmuki, *J. Biomed. Mater. Res. A* 77 (2006) 534.
58. Ramaswamy Narayanan, Hyo-Jin Lee, Tae-Yub Kwon, Kyo-Han Kim, *Materials Chemistry and Physics* 125 (2011) 510.